Minimal Sampling for Effective Acquisition of Anisotropic BRDFs
by R. Vávra & J. Filip

This is the preliminary version of the publication at Pacific Graphics 2016.
The definitive version is available at http://diglib.eg.org/ and http://onlinelibrary.wiley.com.

Pacific Graphics 2016
E. Grinspun, B. Bickel, and Y. Dobashi
(Guest Editors)

*Volume 35 (2016), Number 7*

# Minimal Sampling for Effective Acquisition of Anisotropic BRDFs

R. Vávra† and J. Filip

Institute of Information Theory and Automation of the CAS, Czech Republic

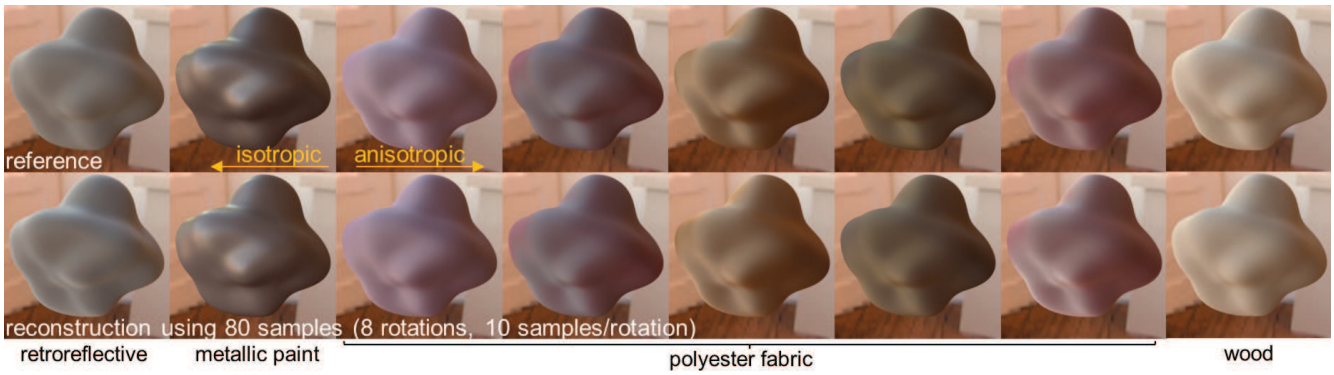


**Figure 1:** *Reconstructed BRDFs using the proposed method from 80 samples.*

**Abstract**

*BRDFs are commonly used for material appearance representation in applications ranging from gaming and the movie industry, to product design and specification. Most applications rely on isotropic BRDFs due to their better availability as a result of their easier acquisition process. On the other hand, anisotropic BRDF due to their structure-dependent anisotropic highlights, are more challenging to measure and process. This paper thus leverages the measurement process of anisotropic BRDF by representing such BRDF by the collection of isotropic BRDFs. Our method relies on an anisotropic BRDF database decomposition into training isotropic slices forming a linear basis, where appropriate sparse samples are identified using numerical optimization. When an unknown anisotropic BRDF is measured, these samples are repeatably captured in a small set of azimuthal directions. All collected samples are then used for an entire measured BRDF reconstruction from a linear isotropic basis. Typically, below 100 samples are sufficient for the capturing of main visual features of complex anisotropic materials, and we provide a minimal directional samples to be regularly measured at each sample rotation. We conclude, that even simple setups relying on five bidirectional samples (maximum of five stationary sensors/lights) in combination with eight rotations (rotation stage for specimen) can yield a promising reconstruction of anisotropic behavior. Next, we outline extension of the proposed approach to adaptive sampling of anisotropic BRDF to gain even better performance. Finally, we show that our method allows using standard geometries, including industrial multi-angle reflectometers, for the fast measurement of anisotropic BRDFs.*

Categories and Subject Descriptors (according to ACM CCS): I.3.7 [Computer Graphics]: Three-Dimensional Graphics and Realism—Color, shading, shadowing, and texture I.4.1 [Computer Graphics]: Digitization and Image Capture—Reflectance

## 1. Introduction

Real-world appearance of spatially homogeneous materials can be represented by means of a bidirectional reflectance distribution function (BRDF) as introduced by Nicodemus et al. [NRH*77]. The BRDF is a four-dimensional vector-valued function $f_r(\theta_i, \varphi_i, \theta_v, \varphi_v)$ of illumination direction $\boldsymbol{I} = [\theta_i, \varphi_i]$ and view direction $\boldsymbol{V} = [\theta_v, \varphi_v]$ that defines how light is reflected at a material's surface for given color channels (see Fig. 2-a). The general four-dimensional function can describe anisotropic materials, i.e., those having variable reflectance when rotated around a surface normal. This property is common for many real-world materials

† vavra@utia.cas.cz

containing any directional elements such as, e.g., thread in fabric, or fiber in wood.

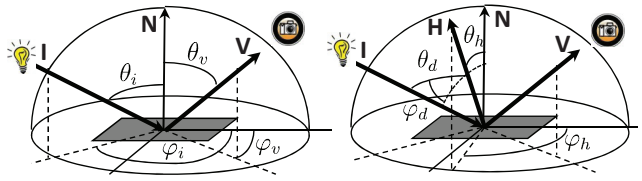


(a) (b)

**Figure 2:** *BRDF parameterizations: (a) spherical, (b) half-difference.*

The three-dimensional simplification of the BRDF neglecting anisotropic appearance is called the isotropic BRDF $f_r(\theta_i, \theta_v, \Delta\varphi = \varphi_v - \varphi_i)$. Despite frequent occurrence of anisotropic materials, little attention has been paid to their proper measurement and representation in past research especially due to a significantly more demanding acquisition process. As one of the challenges of computer graphics remains effective and affordable acquisition of material appearance, any capturing method of anisotropic BRDFs that would leverage this process would benefit many applications.

This paper tackles this goal by capturing few sampling directions for several rotations of the material around its normal, i.e., a measurement process is decomposed into several sparse scans taken at regular azimuthal intervals. Similarly to [NJR15] our data reconstruction relies on material appearance information precomputed from a BRDF database; however, our method is extended to general anisotropic BRDFs. A key principle is the decomposition of training anisotropic BRDFs into a set of isotropic slices in half-difference BRDF parameterization [Rus98], obtained for constant $\varphi_h$. These slices are further used as basis functions describing arbitrary anisotropic behavior without need of its lengthy measurement by regular sampling in the four-dimensional space. Further, we propose a method of significant acceleration of identification of several sparse sets of predefined bidirectional measurement samples taken for each azimuthal scan. The measured BRDF is reconstructed from a linear combination of isotropic slices constrained by measured samples. While the current methods capturing anisotropic appearance require demanding sampling of many different incoming and outgoing directions, the proposed method allows a more practical measurement using a predefined set of fixed sampling directions in combination with sample rotation. Typically less than 10 sampling directions in combination with 8 rotations of the material (80 samples taken together) suffice for reasonable reconstruction of main anisotropic features. The main contributions of this paper are:

- novel effective method for convenient and fast anisotropic BRDF measurement and reconstruction,
- extension of the proposed method to adaptive sampling of material anisotropy,
- a study analyzing ability of industrial multi-angle reflectometers for convenient measurement of anisotropic BRDF using the proposed method.

## 2. Related Work

Our paper relates to BRDF parameterization methods, their measurement and adaptive sampling approaches.

**BRDF data parameterization** holds a key importance in the development of efficient acquisition and rendering algorithms. Depending on the required priority, the data can be organized in a way more suited to certain compression [Rus98] or importance sampling [HFM10] methods. Different parameterizations suggested for several analytic BRDF models are studied in [SAS05]. In this work we focused on half-difference BRDF parameterization [Rus98]. Although this parametrization is inherently anisotropic, it is typically used to represent isotropic materials only.

In our work we use Rusinkiewicz [Rus98] parameterization to decompose anisotropic materials into isotropic slices which are then used as an extensive set of basis functions applicable to efficient measurement and representation of anisotropic BRDFs.

**Anisotropic BRDF measurement** can be split into two groups based on their ability to record material anisotropy or not. However, as the dense measurement of an anisotropic BRDF using gonioreflectometers (as those as in, e.g., [HLZ10, FVH*13]) is very time consuming, setups were developed that reduce the required number of mechanical degrees-of-freedom (DOF). Many setups use mirrors, e.g., kaleidoscopically arranged flat mirrors [HP03], parabolic mirrors [DW04], ellipsoidal mirrors [YSY32], or a combination of concave parabolic and custom-built mirrors [GHAO10]. Another setup used many light sources and sensors [BEWW*08]. They allowed for the capture of many viewing directions simultaneously; however, a limited range of elevation angles resulted. Another group of acquisition methods reduces the number of DOF by using a specimen of a known shape (e.g., spherical, cylindrical or flat). These setups capture either isotropic [MPBM03a] or anisotropic [LL95, NDM05, FVH14] BRDF data. However, accuracy of these measurements is often compromised due to specimens' inhomogeneity and shape imperfections. As a consequence of extensive measurement time, the complexity of setup data calibrations and massive amount of data, there is only a limited number of anisotropic BRDF datasets available. Four of them have been published by Ngan et al. [NDM05] and another three by Filip et al. [FVH14]. Although Ngan's data have minimal azimuthal step $2^o$, they sample four dimensional space relatively sparsely, and are very noisy due to the lower reliability of data captured for higher grazing angles which cause strong visual artifacts when interpolated. Datasets presented in [FVH14] have angular step $2^o$ too, but are already provided interpolated. Despite a high measurement accuracy and precise interpolation, there is still perceptible noise in the data mainly caused by the inhomogeneity of specimens. Recently a database of 150 anisotropic BRDFs was published [FV14] that captures a 4D dataspace uniformly using a relatively low angular resolution of $7.5^o$.

In this paper we propose a novel method of measuring anisotropic BRDFs, based on their decomposition to isotropic slices and leveraging measurement hardware requirements.

**Methods of sparse/adaptive angular measurement** are closely related to our goal as we want to achieve good reconstruction of unknown function by the optimal placement of novel samples based

on previously measured values. This optimal placement depends on a chosen interpolation method. An application of adaptive appearance measurement was investigated in [FBLS07], however, only in two dimensions and representing optimal sampling of the reflectance field. An adaptive approach of image-based BRDF measurement has been proposed in [LLSS03] with planning view and illumination directions based on uncertainty minimization of parameters estimated from the already measured BRDF subspace as represented by the isotropic analytical model. Nauyoks et al. [NFM14] fitted six isotropic BRDF models to the measured data. They iteratively add new measurements by including illumination and view directions where the models differ the most. This method's limitation is that if a certain BRDF model cannot fit measured data reasonably well it has to be excluded from subsequent computation in order to avoid result distraction. Xu et al. [XSD*13] presented anisotropic spherical Gaussians as a closed form representation of anisotropic behavior, that can be practically used for analytical modeling of sparsely sampled BRDF. Recently, Fichet et al. [FSH16] introduced a method fitting locally anisotropic analytic model to sparse measurements transformed to Fourier domain.

**BRDF representation using linear basis** – Matusik et al. [MPBM03b] represented a database of isotropic BRDFs using wavelet-basis and the linear combination of BRDFs. Similarly, Nöll et al. [NKS14] represented the database using basis functions, however, their reconstruction's deviations from the reference were approximated by basis of correction functions. Another approach uses precomputed optimized sampling patterns of all recorded anisotropic BRDFs in database [FV14]. When new material is measured, the closest sampling template is found based only on a very sparse set of measurements. Such a template is either directly used for sampling the BRDF, or is dynamically switched over the course of measurement. Nielsen et al. [NJR15] presented an approach reconstructing isotropic BRDFs from basis functions using extremely sparse measurements. This approach can optimize a set of appropriate directional samples based on the information from the database; however, it cannot achieve any adaptivity towards the measured samples.

Our goal is to extend methods based on a linear basis [MPBM03b], [FV14], [NJR15] to efficient adaptive sampling solely in an anisotropic domain.

## 3. Proposed Measurement Method

A key principle of our method is the decomposition of each anisotropic BRDF into a set of their isotropic BRDFs, so called slices, independent of material rotation around its normal, i.e., the slices are independent of azimuthal parameter $\varphi_h$. The measured anisotropic material can then be sampled in a very limited number of sampling directions for several rotations around its normal and accurately reconstructed. The reconstruction relies on principal components formed from the anisotropic BRDF database.

### 3.1. Linear Basis Formation

As the number of publicly available anisotropic BRDFs is limited, we resorted to the UTIA BRDF Database http://btf.utia.cas.cz presented in [FV14] as the only source of a reasonable number of different types of anisotropic BRDF measurements. This database contains 150 BRDFs of fabric, wood, leather, plastic and paint materials; out of which, over 40 exhibit some strong visual aspect of anisotropy as discussed in [Fil15]. The BRDFs are stored in HDR format, and their angular resolution is $15^o$ in elevations and $7.5^o$ in azimuthal angles.

We use BRDF in half-difference (HD) parameterization and generate linear basis similarly to [NJR15]. This parameterization proposes the change of variables from $f_r(\theta_i,\varphi_i,\theta_v,\varphi_v)$ to $f_r(\theta_h,\varphi_h,\theta_d,\varphi_d)$ as show in Fig. 2-b. The BRDF is represented by a halfway vector $\mathbf{H}$ between the illumination and viewing directions, and by the difference vector $\mathbf{D}$, which is the illumination direction in a coordinate system related to the halfway vector. Thus, the halfway vector is parameterized by spherical angles $\boldsymbol{H} = [\theta_h,\varphi_h]$ with respect to the sample's normal, and the illumination direction $\mathbf{D}$ is parameterized by spherical angles $\boldsymbol{D} = [\theta_d,\varphi_d]$ with respect to the halfway vector. Therefore, the anisotropic BRDF in this parameterization is represented by a four-dimensional function $f_r(\theta_h,\varphi_h,\theta_d,\varphi_d)$, where $(\theta_h,\theta_d) \in [0,\frac{\pi}{2}]$, $\varphi_h \in [0,2\pi)$, and $\varphi_d \in [0,\pi)$. The isotropic BRDFs can be described by its three-dimensional variant $f_r(\theta_h,\theta_d,\varphi_d)$.

As the anisotropic database is provided in a standard parameterization, we converted it to HD parameterization with uniform sampling step $5^o$ in all dimensions. We verified that due to initial resolution of the database, this sampling step is sufficient to capture all visual features in original BRDFs. The benefit of non-linear sampling along $\theta_h$, proposed by Matusik et al. [MPBM03a], is negligible in this case as the database does not contain any extremely specular material. In this step, each anisotropic BRDF was decomposed into $n_{\varphi_h} = 360^o/5^o = 72$ isotropic slices $f_{iso}$ per color channel. As we treat color channels independently, we obtain 3·72 = 216 isotropic BRDF slices per each material.

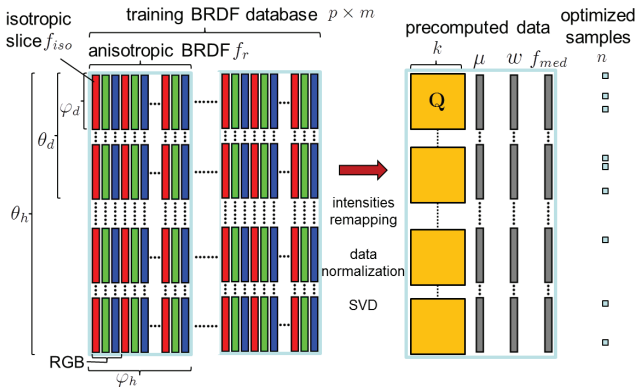


**Figure 3:** *Overview of input BRDF data arrangement and precomputed data products necessary for BRDF reconstruction.*

Values of these isotropic BRDFs $f_{iso}$ depending on parameters $\varphi_d$, $\theta_d$, and $\theta_h$ are vectorized and stacked together to form a matrix $\boldsymbol{A} \in \mathbb{R}^{p\times m}$ whose structure is depicted in Fig. 3 and where $p = n_{\varphi_d} \cdot n_{\theta_d} \cdot n_{\theta_h} = 36 \cdot 18 \cdot 18 = 11,664$ is number of rows and $m = 3 \cdot n_{\varphi_h} \cdot 150 = 32,400$ is number of columns as there are 150 materials in the BRDF database.

Now, we can remap the data intensities as suggested in [NJR15].

First, we compute a median isotropic BRDF $f_{med}$ across all $m$ columns of $\boldsymbol{A}$ and a cosine-weight factor compensating for low grazing-angle values $\boldsymbol{w} = \max\{\cos\theta_i \cos\theta_v, \varepsilon\}$, where $\varepsilon = 0.001$ is a constant guaranteeing numerical stability. Then, we remap the data forming matrix $\boldsymbol{X} \in \mathbb{R}^{p\times m}$, whose each element is computed as:

$$X_{a,b} = \ln\left(\frac{A_{a,b}\cdot w_a + \varepsilon}{f_{med,a}\cdot w_a + \varepsilon}\right), \forall a \in \{1,\dots,p\}, \forall b \in \{1,\dots,m\}. \tag{1}$$

Next, we subtract the mean $\boldsymbol{\mu}$ over columns of matrix $\boldsymbol{X}$ introducing matrix

$$\boldsymbol{Y} = \boldsymbol{X} - \boldsymbol{\mu}\cdot\boldsymbol{J}_{1,m} \ , \tag{2}$$

where $\boldsymbol{J}_{a,b}$ is matrix of ones of size $a\times b$, replicating column vector $\boldsymbol{\mu}$ m-times.

Finally, linear basis is derived by applying singular value decomposition (SVD) to matrix $\mathbf{Y}$:

$$\boldsymbol{Y} = \boldsymbol{U}\boldsymbol{\Sigma}\boldsymbol{V}^T \ ,$$

where columns of matrix $\boldsymbol{U}$ are principal components of the data. Note that the decomposition can be performed based on eigenvectors of $\boldsymbol{Y}^T\boldsymbol{Y}$ or $\boldsymbol{Y}\boldsymbol{Y}^T$ to save computational time. We keep here the same notation as [NJR15] and define matrix $\boldsymbol{Q} \in \mathcal{R}^{p\times k}$ of principal components weighted by the variance they cover as

$$\boldsymbol{Q} = \boldsymbol{U}\Sigma \ ,$$

where $k \le m$ is number of applied principal components.

### 3.2. Data Reconstruction

Our goal is to reconstruct the missing elements of the measured BRDF, given the small number of samples $n$ for each of $r$ rotations. For simplicity, assume $r = n_{\varphi_h} = 72$, e.i., we are given values for the same number of rotations as in the database. Later, we describe how to manage situations where $r < n_{\varphi_h}$.

Let $\tilde{\boldsymbol{A}} \in \mathbb{R}^{n\times r}$ be the matrix of known values of a reconstructed BRDF, let $\tilde{f}_{med} \in \mathbb{R}^n$ be the vector of corresponding median values, let $\tilde{\boldsymbol{w}} \in \mathbb{R}^n$ be the vector of corresponding weights, and let $\tilde{\boldsymbol{\mu}} \in \mathbb{R}^n$ be the vector of corresponding mean values. Applying those as in Equation 1 and 2 respectively, we obtain matrix $\tilde{\boldsymbol{Y}} \in \mathbb{R}^{n\times r}$. Let $\tilde{\boldsymbol{Q}} \in \mathbb{R}^{n\times k}$ be the corresponding rows of the principal components in $\boldsymbol{Q}$. Then, matrix $\boldsymbol{C} \in \mathbb{R}^{k\times r}$ of coefficients of the linear combination of principal components that best models the observed data is obtained by:

$$\begin{aligned}
\tilde{\boldsymbol{Y}} &= \tilde{\boldsymbol{Q}}\boldsymbol{C} \\
\boldsymbol{C} &= \arg\min_{\boldsymbol{C}} E(\boldsymbol{C}) \\
E(\boldsymbol{C}) &= \|\tilde{\boldsymbol{Y}} - \tilde{\boldsymbol{Q}}\boldsymbol{C}\|_F^2 \\
\boldsymbol{C} &= (\tilde{\boldsymbol{Q}}^T\tilde{\boldsymbol{Q}})^{-1}\tilde{\boldsymbol{Q}}\tilde{\boldsymbol{Y}}.
\end{aligned}$$

Notice that in this case individual columns of $\mathbf{C}$ can be computed separately. The full remapped BRDF, $\bar{\boldsymbol{X}} \in \mathbb{R}^{p\times r}$, is then reconstructed by using the full principal components:

$$\bar{\boldsymbol{X}} = \boldsymbol{Q}\cdot\boldsymbol{C} + \boldsymbol{\mu}\cdot\boldsymbol{J}_{1,r}, \tag{3}$$

where $\boldsymbol{J}_{a,b}$ is matrix of ones of size $a\times b$. Then, we obtain the full reconstructed BRDF, $\bar{\boldsymbol{A}} \in \mathbb{R}^{p\times r}$, by application of inverse mapping of Equation 1 to each element:

$$\bar{A}_{a,b} = \frac{e^{\bar{X}_{a,b}}(f_{med,a}\cdot w_a + \varepsilon) - \varepsilon}{w_a}, \forall a \in \{1,\dots,p\}, \forall b \in \{1,\dots,r\}.$$

Nielsen et al. [NJR15] noticed, that the least squares solution above usually results in over-fitted results, deviating significantly from ground truth. Therefore, they proposed a biased solution based on the work of Blanz et al. [BMVS04], who claimed that $\|C\|_F^2$ is proportional to the unlikelihood of a reconstruction. By means of introduction of the Lagrange multiplier $\eta$ in conjunction with the Frobenius norm of $\boldsymbol{C}$, it is possible to favor reconstructions closer to the observed distribution of BRDFs:

$$\begin{aligned}
E(\boldsymbol{C}) &= \|\tilde{\boldsymbol{Y}} - \tilde{\boldsymbol{Q}}\boldsymbol{C}\|_F^2 + \eta\|\boldsymbol{C}\|_F^2 \\
\boldsymbol{C} &= (\tilde{\boldsymbol{Q}}^T\tilde{\boldsymbol{Q}} + \eta\boldsymbol{I})^{-1}\tilde{\boldsymbol{Q}}\tilde{\boldsymbol{Y}},
\end{aligned} \tag{4}$$

where $\boldsymbol{I}$ is the identity matrix.

When this method is applied for reconstruction of anisotropic data, we have to keep in mind, that a value of the BRDF in specular reflection ($\theta_h = 0$) does not change when only $\varphi_h$ change as it is undefined there, but the function values must meet in specular reflections. Therefore, if $\theta_{h,a} = \theta_{h,b} = 0$, $\theta_{d,a} = \theta_{d,b}$, and $\varphi_{d,a} = \varphi_{d,b}$ then $f_r(\theta_{h,a},\varphi_{h,a},\theta_{d,a},\varphi_{d,a}) = f_r(\theta_{h,b},\varphi_{h,b},\theta_{d,b},\varphi_{d,b})$ must hold $\forall a,b \in \{1,\dots,p\}$. In other words, all isotropic slices $\bar{f}_{iso}$ of the reconstructed material belonging to the same color channel must have the same value on the rows where $\theta_h = 0$, i.e., $\bar{A}_{c,a} = \bar{A}_{c,b}, \forall c \in \{1,\dots,p\}$ where $\theta_h = 0, \forall a,b \in \{1,\dots,r\}$. This condition is key in our model as data are tabulated and modeled independently of $\varphi_h$ or else there are perceptible artifacts around specular reflections in reconstructed BRDFs.

Let $\tilde{\tilde{\boldsymbol{Q}}} \in \mathbb{R}^{s\times k}$ be a matrix of the rows of the principal components in $\boldsymbol{Q}$ satisfying condition above, i.e., the rows where $\theta_h = 0$, where $s$ is number of the rows satisfying the condition (in our case $s = n_{\varphi_d}\cdot n_{\theta_d} = 36\cdot 18 = 648$). To satisfy the condition we introduce another Lagrange multiplier $\lambda$ in conjunction with the Frobenius norm of residual after subtracting its mean from reconstruction of the involved rows:

$$\begin{aligned}
E(\boldsymbol{C}) &= \|\tilde{\boldsymbol{Y}} - \tilde{\boldsymbol{Q}}\boldsymbol{C}\|_F^2 + \eta\|\boldsymbol{C}\|_F^2 + \lambda\|\tilde{\tilde{\boldsymbol{Q}}}\boldsymbol{C} - \mathbf{v}\cdot\boldsymbol{J}_{1,r}\|_F^2 \\
&= \|\tilde{\boldsymbol{Y}} - \tilde{\boldsymbol{Q}}\boldsymbol{C}\|_F^2 + \eta\|\boldsymbol{C}\|_F^2 + \lambda\|\tilde{\tilde{\boldsymbol{Q}}}\boldsymbol{C} - \frac{1}{r}\cdot\tilde{\tilde{\boldsymbol{Q}}}\boldsymbol{C}\boldsymbol{J}_{r,r}\|_F^2 \\
&= \|\tilde{\boldsymbol{Y}} - \tilde{\boldsymbol{Q}}\boldsymbol{C}\|_F^2 + \eta\|\boldsymbol{C}\|_F^2 + \lambda\|\tilde{\tilde{\boldsymbol{Q}}}\boldsymbol{C}\boldsymbol{M}\|_F^2,
\end{aligned} \tag{5}$$

where $\mathbf{v}$ is a column vector of mean values of rows of a matrix $\tilde{\tilde{\boldsymbol{Q}}}\boldsymbol{C}$, and $\boldsymbol{M} = \boldsymbol{I} - \frac{1}{r}\cdot\boldsymbol{J}_{r,r}$. Equation 5 has no close form solution and must be optimized numerically. During optimization, we can at least use its gradient, whose detailed derivation is in Appendix A:

$$\nabla E(\boldsymbol{C}) = -2\tilde{\boldsymbol{Q}}^T\boldsymbol{Y} + 2\tilde{\boldsymbol{Q}}^T\tilde{\boldsymbol{Q}}\boldsymbol{C} + 2\eta\boldsymbol{C} + 2\lambda\tilde{\tilde{\boldsymbol{Q}}}^T\tilde{\tilde{\boldsymbol{Q}}}\boldsymbol{C}\boldsymbol{M}\boldsymbol{M}.$$

In our implementation, we first estimate $\boldsymbol{C}$ using Equation 4 and then we perform unconstrained minimization (Matlab function fminunc) to find the local optimum of Equation 5. We found the method best works on our dataset for parameter values $\eta = 40$ and $\lambda = 0.1$. As we remove color information from the data during the formation of matrix $\boldsymbol{A}$ (see Section 3.1 and Figure 3), coefficients $\boldsymbol{C}$ for each color channel must be computed separately.

Now, we describe how to handle situations where the number of rotations $r$ of the measured material around its normal is smaller than that of original data $n_{\varphi_h}$. There are three possible solutions. The first relies on interpolation of the measured data to the required resolution by Piecewise Cubic Hermite Interpolating Polynomials (PCHIP) producing periodic interpolated functions. The second approach is based on the similar interpolation of the linear coefficients $\boldsymbol{C}$. Although the second approach is faster, as it evaluates significantly lower number of variables in Equation 5, it produces slightly worse results. Moreover, the second approach cannot be used when we do not measure all sampling directions in each of the material's rotations. We used the second approach as it is much faster, unless for adaptive sampling (Section 6) where the first one was used. The third approach is a simple interpolation of reconstructed BRDF $\tilde{\boldsymbol{A}}$.

### 3.3. Optimization of Sampling Directions

To identify optimal sampling directions we follow an approach of Matusik et al. [MPBM03b] improved by Nielsen et al. [NJR15]. Let us recall that a measured BRDF is reconstructed by Equation 3 using matrix $\boldsymbol{C}$ of coefficients of the linear combination of principal components $\boldsymbol{Q}$. Computation of coefficients $\boldsymbol{C}$ by means of Equation 5 is highly dependent on subset of rows of principal components $\tilde{\boldsymbol{Q}}$ that corresponds to selected sampling directions. To minimize sensitivity to errors in the modeling we need to select the subset with minimal condition number $\kappa$ for given count of samples $n$. Condition number $\kappa$ is defined as a ratio of maximal singular value of $\tilde{\boldsymbol{Q}}$ and minimal singular value of $\tilde{\boldsymbol{Q}}$. Similarly to Nielsen et al. [NJR15] we exploit the fact that we are dealing with three dimensional BRDF volume $(\varphi_d, \theta_d, \theta_h)$ whose each location corresponds to one row in $\boldsymbol{Q}$. We slightly modified approach of Nielsen et al. [NJR15] and propose the following algorithm:

1. Pick $n$ random sampling locations in $(\varphi_d, \theta_d, \theta_h)$, i.e. pick $n$ random rows of $\boldsymbol{Q}$ forming $\tilde{\boldsymbol{Q}}$. Based on our experience, even random selection with extremely high $\kappa(\tilde{\boldsymbol{Q}})$ might lead to a good solution. Save $\tilde{\boldsymbol{Q}}$ for a later usage in step 4.
2. Randomly choose one of the $n$ rows and exclude it from matrix $\tilde{\boldsymbol{Q}}$ forming matrix $\bar{\boldsymbol{Q}}$. For each location in $(\varphi_d, \theta_d, \theta_h)$ in excluded location's neighborhood of size $h \times h \times h$ evaluate condition numbers efficiently using method described in Appendix B based on eigenvectors and eigenvalues of $\bar{\boldsymbol{Q}}^T \bar{\boldsymbol{Q}}$. Accept location with the lowest $\kappa$ if it is lower than the current $\kappa$.
3. Repeat from 2. until convergence.
4. Restore the original $\tilde{\boldsymbol{Q}}$ and repeat from 2. 10-times.
5. Repeat from 1. 10-times.

We use neighborhood of size $h = 7$. Thanks to the method of a fast updating of singular values when adding one row to a matrix described in Appendix B, we can search the neighborhood of a current location very quickly; we can find better solution in a given amount of time. When compared to standard approach to conditional numbers computation, the proposed method's speed gain is $2\times$ for $n = 5$, $4\times$ for $n = 20$, and $15\times$ for $n = 50$.

Optionally, we can even search the whole space and place the excluded sampling location to an optimal position with respect to the other sampling locations. Unfortunately, this approach does not lead to better solutions than the algorithm described above and is rather slower.

## 4. Results

This section presents results of the proposed sparse measurement and reconstruction method on database of 150 anisotropic BRDFs. We used this dataset as our reference data, and any errors introduced by our methods were evaluated using logarithmic PSNR (log PSNR) HDR measure presented by Tunc et al. [AMS08]. To avoid sharing the same training and testing data, we applied leave-one-out validation, i.e., excluding each tested BRDF's data from the linear base.

Fig. 4 shows the error averaged across all materials from database as a function of total number of samples. The outlines in the graph (a) depict different number of samples per rotations $n = 2, 5, 10, 20, 50, 100$, while in graph (b) it shows variable number of rotations $r = 4, 8, 12, 24, 36, 72$. From the graphs we can draw a conclusion that in general, $n$ has greater impact on reconstruction error than $r$, where minimal improvement is achieved for more that $r = 12$ rotations. One can observe rapid decrease of error when

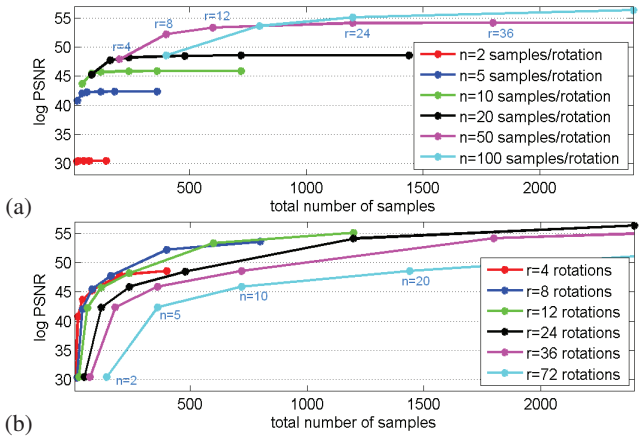


**Figure 4:** *The reconstruction error (log PSNR) as a function of total number of samples for individual tested samples per rotation n and number of rotations r (higher is better).*

eight or more rotations were used. Similarly, the error drops for five to ten samples per rotation; whereas, for more the improvement is approximately linear to the number of samples. Therefore, an ideal measurement method should decompose measurement into 8 rotations and number of samples taken for each rotation should be selected up on accuracy requirements starting from $n = 5$. Visual results for selected materials for configurations $n = 5/r = 8$ (40 samples) and $n = 10/r = 8$ (80 samples) are shown for point-light illumination in Fig. 9 and for environment illumination in Fig. 1. The remaining ones are shown in a supplementary material.

Fig. 5 presents the reconstruction errors across all 150 tested materials from the database for (a) 10 samples per rotation and various number of rotations, and (b) 8 rotations and various numbers of samples per rotation. Here again one can clearly observe that the impact of the number of samples per rotation is more significant.

For visual comparison we used a surface optimized to high coverage of illumination and viewing angles proposed by Havran et al. [HFM16]. We rendered such a surface for the defined optimized

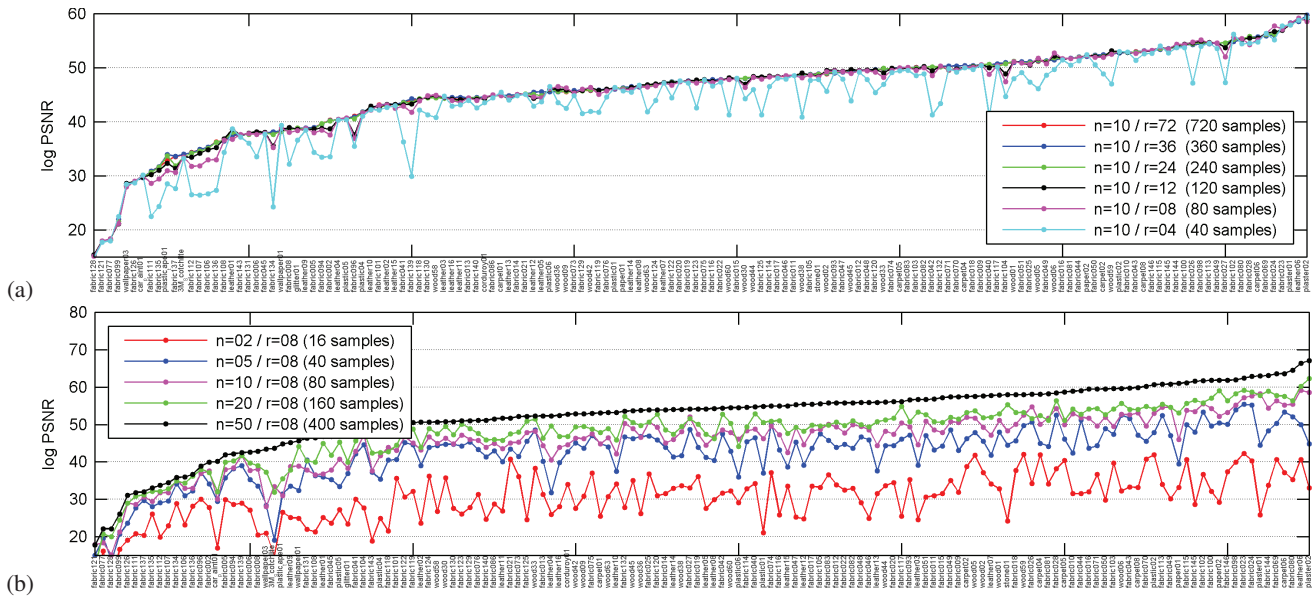


**Figure 5:** *BRDF reconstruction error (log PSNR) for 150 tested materials: (a) for fixed number of samples per rotation $n = 10$, (b) for fixed number of rotations $r = 8$.*

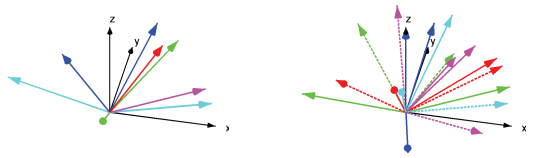

| 5 samples | | | 10 samples | | | | | |
|---|---|---|---|---|---|---|---|---|
| $\theta_h$ | $\theta_d$ | $\varphi_d$ | $\theta_h$ | $\theta_d$ | $\varphi_d$ | $\theta_h$ | $\theta_d$ | $\varphi_d$ |
| 30 | 0 | 130 | 35 | 50 | 55 | 15 | 60 | 35 |
| 0 | 30 | 40 | 25 | 70 | 95 | 0 | 0 | 0 |
| 35 | 60 | 75 | 0 | 75 | 15 | 0 | 30 | 165 |
| 0 | 75 | 0 | 15 | 40 | 80 | 75 | 0 | 0 |
| 65 | 0 | 0 | 35 | 10 | 65 | 30 | 50 | 140 |

**Figure 6:** *Optimized sampling directions for $n = 5$ and $n = 10$ samples per rotation. All values are in degrees.*

positions of light and camera for different combinations of parameters $n = 5, 10, 20$ and $r = 4, 8, 12$. Fig. 8 shows, accordingly to the previous results, the significant performance gain when more than four rotations and 10 samples per rotation are used. For more materials and settings combinations please refer to the supplementary material. Visualization of eight materials under environment illumination is shown in Fig. 1. The optimized directions for $n = 5, 10$ are shown in Fig. 6.

Finally, we compared our method with another recent approaches to adaptive sampling of anisotropic BRDFs presented in [FV14]. Fig. 7 illustrates that the proposed method performs significantly better then template-based approaches (*method 1*, *method 2*) when total number of samples drops under 500. One can observe that method based on linear basis, however, selecting the samples globally (*lin.comb.*) [MPBM03b] achieves slightly higher PSNR values. Note that our method uses the regularization constraint [NJR15] that avoids data over-fitting at the cost of slightly lower PSNR values. Thus, PSNR values of *lin.comb.* might not always correspond to visual performance.

## 5. Discussion and Limitations

**Contribution of the proposed optimization constraint** – the original optimization approach produces disruptive anisotropic artifacts running from the singularity point ($\theta_h = 0$) and interfering with the anisotropic highlight. Figure 10 compares the contribution of the proposed constrained optimization according Equation 5 when compared to the original approach (Equation 4) on a sphere. While the original approach achieves overall higher PSNR than the constrained approach, it introduces the aforementioned anisotropic artifacts.

**Linear basis formed by isotropic slices vs. full BRDFs** – alternatively to our approach one can optimize sampling directions simultaneously over full four-dimensional BRDF space. We com-

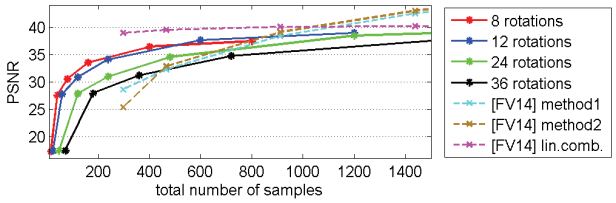


**Figure 7:** *The reconstruction error (PSNR) as a function of total number of samples for variants of the proposed method and methods presented in [FV14].*

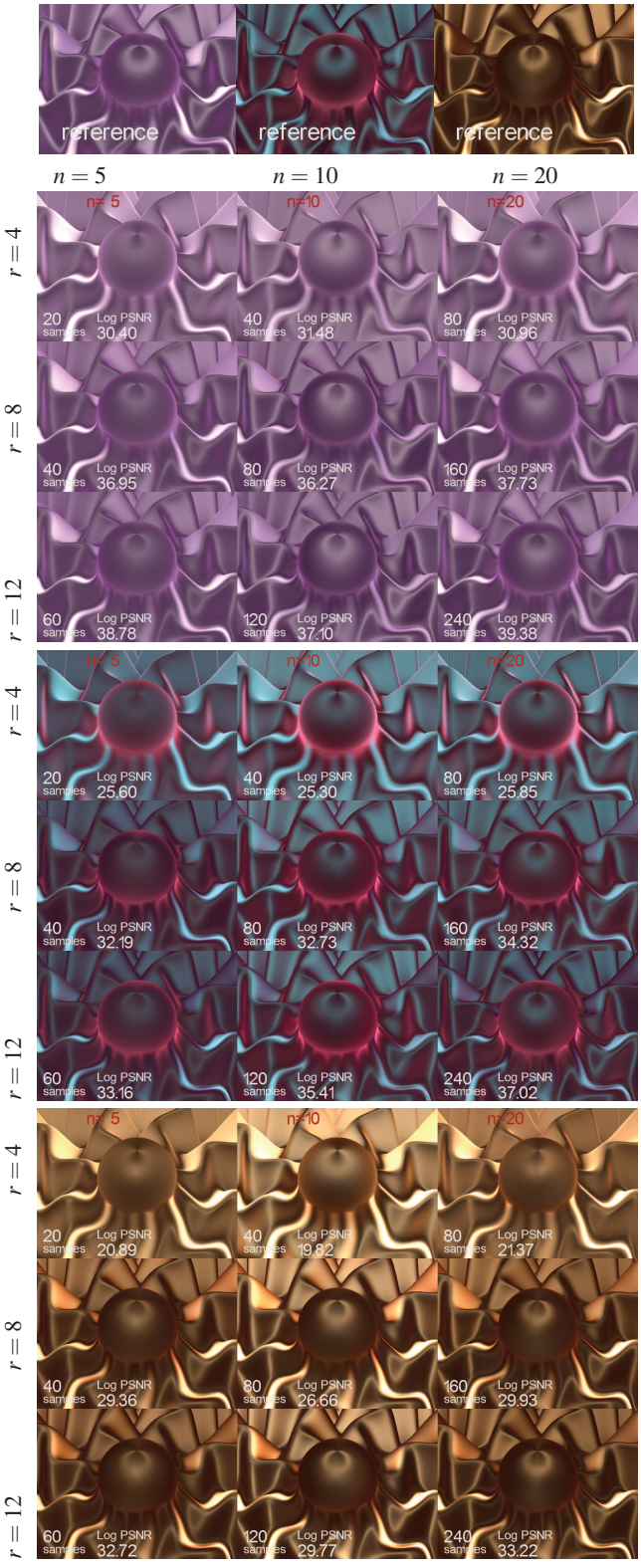


**Figure 8:** *Rendering of reconstructed BRDF for three anisotropic BRDFs as a function of number of samples per rotation n (columns), and number of rotations r (rows). Included are values of Log PSNR error and total number of samples taken.*

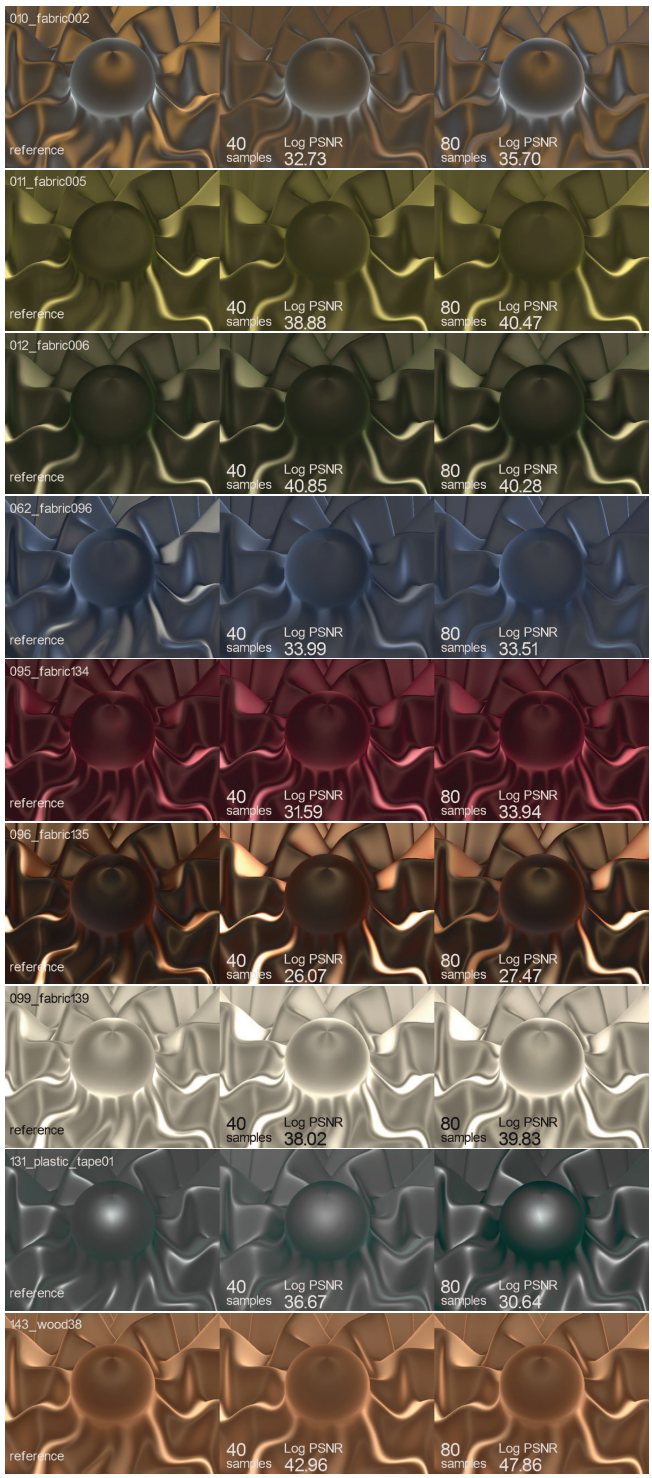


**Figure 9:** *Results of the proposed method on selected anisotropic materials from the database for configurations using: 40 samples, i.e. $n = 5/r = 8$ (middle), and 80 samples, i.e. $n = 10/r = 8$ (right). Included are values of Log PSNR against the reference (left).*

(a) original optimization [NJR15]

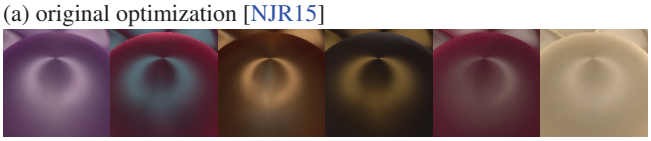

(b) optimization using the proposed regularization constraint

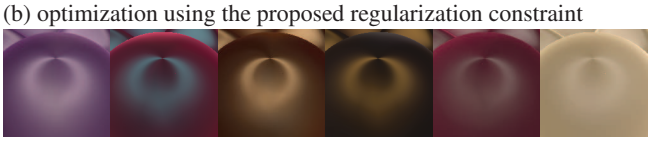

**Figure 10:** *Comparison of parameters optimization approaches: (a) original optimization according Eq. 4, (b) proposed constrained optimization according Eq. 5. Parameters used $n = 10$ / $r = 36$, 360 samples.*

pared to this approach in Fig. 7. Although the idea seems appealing it has several drawbacks. First, our method, in comparison with other anisotropic sampling approaches [FV14], does not require any azimuthal alignment of the material during the measurement process. This saves up to 48 samples that were previously needed for an anisotropic axes identification. Second, this approach would require much bigger database of anisotropic BRDFs as the datavectors would have one order of magnitude higher dimensionality. The insufficient number of datasets results in various color artifacts present in the reconstructed BRDFs [FV14]. Third, using the full BRDFs would not allow the proposed fast measurement of anisotropic BRDF by a simple rotation of the precomputed sampling directions.

**Training datasets limits** – As any machine learning method our approach is limited mainly by descriptiveness of the training dataset. Therefore, a collection of anisotropic materials of various appearance behavior is necessary. An example of insufficient training data is highly retro-reflective material *3M_Scotchlite*, where performance of our method is not ideal (the first material in Fig. 1) as it is the only material of this kind in the database. We tested sensitivity of the reconstruction quality to filtering of BRDFs used for formation of the linear basis, i.e., selection of the subset of the most similar isotropic BRDFs. We used a technique based on similarity between the captured sparse samples of the query material, and the isotropic slices stored in the basis. Although there was a noticeable effect of this filtering the final performance gain was negligible when considered increased computational costs related to such customized linear basis formation. One may consider also adding MERL isotropic BRDFs [MPBM03a] to expand our basis. Our experience shows that using isotropic data as the only basis is insufficient as such data miss unique features occurring in anisotropic BRDFs only. On the other hand, their addition to the basis might improve the performance, although one have to carefully resample any added BRDF into resolution of BRDF basis.

**Reconstruction accuracy** – our experiments revealed that typically the highest BRDF reconstruction errors occur for grazing angles, i.e. around object contours (see rendering difference images in the supplementary). This corresponds to the angles where a BRDF has the highest energy.

In the applied context of the measurement process, one may require information how well the available linear base represents the material being measured. To this end, we evaluated the mean reconstruction error only in the samples measured and compared its correlation with the error evaluated across entire BRDF. The correlation value depend on combination $n$ and $r$, however, above $n \geq 10$ and $r \geq 8$ the Pearson correlation coefficient was over 0.9. Thus, relation of the errors over the 150 tested materials can be approximately represented by a single scaling factor 0.8, i.e., one should multiply the mean error obtained in sampling locations to estimate a reconstruction error of entire BRDF, providing an approximate level of certainty whether the material is properly represented by the limited linear base.

**Timings** – our method was implemented in MATLAB and all processing was done on a CPU Intel Xeon E5-2643. The computation of linear basis consisting of 32,400 isotropic BRDF slices took approximately four minutes. Identification of 20 optimized directions took three minutes. Note that these two steps have to be performed only once while the anisotropic reconstruction from measured sparse samples for configuration $n$=20 / $r$=12 takes ≈1.5 seconds and for $n$=20 / $r$=72 takes 14 seconds.

## 6. Adaptive Measurement of Anisotropy

Our technique captures anisotropic appearance by a set of regularly spaced rotations of the measured sample. Another performance gain can be achieved by coarse regular sampling combined with further refinement using adaptive placement of another rotations in an arbitrary step. This method can be easily applied once the remotely controlled rotation stage is used. The method enables increasing measurement quality while preserving or even decreasing measurement time. The process of adaptive measurement is as follows:

1. Capture BRDF with sparse azimuthal sampling (e.g. 8 rotations).
2. For each captured sample respectively evaluate BRDF reconstruction error by interpolating its value based on captured samples in its neighborhood using piecewise cubic hermite interpolating polynomial (Matlab function pchip).
3. If interpolated and actual value of the sample differs more than $e$ percent, plan to measure two sampling directions: the middle point between the sample and its left neighbor, and the middle point between the sample and its right neighbor.
4. Capture all planed sampling directions and repeat from 2. until all errors are lower than $e$ percent.

Fig. 11 shows dependency of a total number of samples and BRDF reconstruction error on adaptive threshold $e$ for fixed number of initial rotations $r = 8$. The horizontal dashed lines depict results of non-adaptive regular sampling of anisotropy using $r = 8$ rotations. The best trade-off between number of samples and reconstruction quality is achieved when threshold $e = 0.1$ is used.

Fig. 12 illustrates visual fidelity gain achieved by adaptive placement of rotations. One can observe significant improvement while only 70 samples placed adaptively is used instead of the 80 samples placed over uniformly distributed rotations. Rendered results illustrating performance of adaptive sampling as a function of $n$

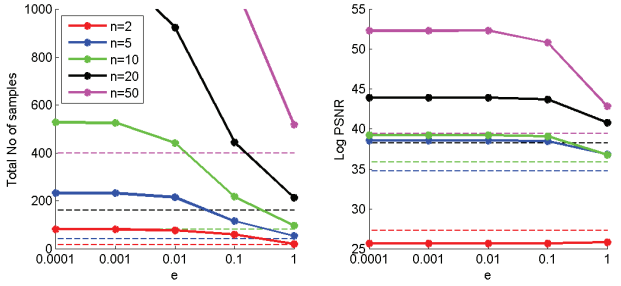


**Figure 11:** *A total number of samples and reconstruction error averaged over six highly anisotropic materials (see Fig. 1) as a function of adaptive threshold e for fixed number of initial rotations* $r = 8$.

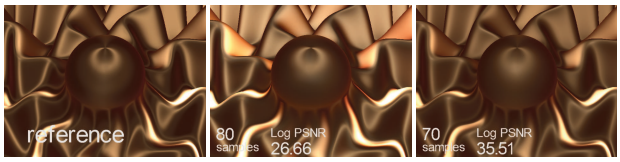


(a) (b) non-adaptive (c) adaptive

**Figure 12:** *An example of contribution gained by adaptive measurement of highly anisotropic material* fabric111*: (a) reference, (b) non-adaptive measurement using 80 samples (*$r = 8$ */* $n = 10$*), (c) adaptive measurement using 70 samples (*$n = 5$*,* $e = 1.0$*, initial number of rotations* $r = 8$*).*

**Table 1:** *The geometries sampled by the industrial devices in the standard BRDF parametrization. All values are in degrees.*

| MA68 | | | | MA98 | | | | BYK-mac | | | | Multi FX10 | | | |
|---|---|---|---|---|---|---|---|---|---|---|---|---|---|---|---|
| $\theta_i$ | $\varphi_i$ | $\theta_v$ | $\varphi_v$ | $\theta_i$ | $\varphi_i$ | $\theta_v$ | $\varphi_v$ | $\theta_i$ | $\varphi_i$ | $\theta_v$ | $\varphi_v$ | $\theta_i$ | $\varphi_i$ | $\theta_v$ | $\varphi_v$ |
| in-plane samples | | | | | | | | | | | | | | | |
| 45 | 0 | 0 | 0 | 45 | 0 | 0 | 0 | 45 | 0 | 0 | 0 | 45 | 0 | 0 | 0 |
| 45 | 0 | 30 | 0 | 45 | 0 | 30 | 0 | 45 | 0 | 30 | 0 | 45 | 0 | 30 | 0 |
| 45 | 0 | 65 | 0 | 45 | 0 | 65 | 0 | 45 | 0 | 65 | 0 | 45 | 0 | 65 | 0 |
| 45 | 0 | 20 | 180 | 45 | 0 | 20 | 180 | 45 | 0 | 20 | 180 | 45 | 0 | 20 | 180 |
| 45 | 0 | 30 | 180 | 45 | 0 | 30 | 180 | 45 | 0 | 30 | 180 | 45 | 0 | 30 | 180 |
| | | | | 45 | 0 | 60 | 180 | 45 | 0 | 60 | 180 | 45 | 0 | 60 | 180 |
| | | | | 15 | 0 | 30 | 0 | | | | | 15 | 0 | 0 | 180 |
| | | | | 15 | 0 | 65 | 0 | | | | | 15 | 0 | 30 | 180 |
| | | | | 15 | 0 | 20 | 180 | | | | | 65 | 0 | 50 | 180 |
| | | | | 15 | 0 | 30 | 180 | | | | | 65 | 0 | 80 | 180 |
| | | | | 15 | 0 | 60 | 180 | | | | | | | | |
| out-of-plane samples | | | | | | | | | | | | | | | |
| | | | | 15 | 0 | 50 | 33 | | | | | | | | |
| | | | | 15 | 0 | 50 | 327 | | | | | | | | |
| | | | | 15 | 0 | 45 | 90 | | | | | | | | |
| | | | | 15 | 0 | 45 | 270 | | | | | | | | |
| | | | | 45 | 0 | 50 | 33 | | | | | | | | |
| | | | | 45 | 0 | 50 | 327 | | | | | | | | |
| | | | | 45 | 0 | 45 | 90 | | | | | | | | |
| | | | | 45 | 0 | 45 | 270 | | | | | | | | |
| 5 samples | | | | 19 samples | | | | 6 samples | | | | 10 samples | | | |

and $e$ are shown in the supplementary material. Although adaptive sampling of $\varphi_h$ is more technically demanding, but when remotely controlled rotation stage is used one can achieve better results using a more simple and thus less expensive setup (as shown in Fig. 12).

## 7. Measurement by Multi-Angle Reflectometers

The proposed method allows capturing anisotropic appearance by very low number of bidirectional pairs of lights and sensors. As these pairs are taken identically for each rotation of the measurement geometry, one can develop a relatively simple setup for measurement of material appearance.

Before building any new setup, one can validate current industrial standards used for the measurement of appearance [WM01] and test current devices used in industry for multi-angle reflectance measurement. To this end, we tested bidirectional pairs configurations corresponding to four common industrial devices: MA68 and MA98 by X-rite, BYK-mac by Gardner, and MultiFX10 by Datacolor as described more in detail in [PCVMV13]. These devices typically take between 5-11 in-the-plane measurements to identify unique reflectance properties of materials as shown in Tab 1. Only MA98 use eight additional out-of-plane bidirectional pairs. Note that the first five in-plane samples, stemming from ASTM and DIN standards [WM01], are captured by all evaluated devices.

In the context of our work, one can directly use only the pairs specified by the device for BRDF reconstruction instead of optimized bidirectional pairs. Capturing anisotropy can be achieved either by the repositioning of the device above material or by material rotation below the device. Fig. 13 shows the results averaged across 150 BRDFs, obtained when compared with various numbers of optimized directions ($n = 5, 10, 20$) as a function of material's rotation number. The graph shows comparable performance of the setups with the proposed sampling for low samples numbers (MA68, BYK-mac); however, with the increasing number of samples the best reconstruction quality is obtained by means of using optimized directions. The best trade-off between reconstruction error and number of rotations is obtained at eight rotations.

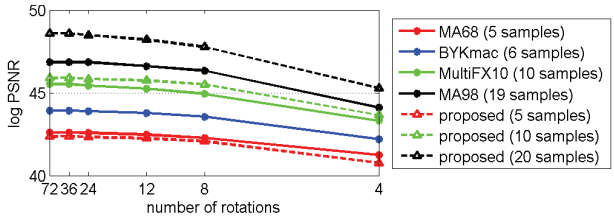


**Figure 13:** *A comparison of average BRDF reconstruction quality from 5 and 10 optimized samples with reconstruction from samples taken by industrial appearance capturing devices, as a function of number of surface rotations.*

However, when we focus on highly anisotropic materials, representing main measurement challenges of this paper, it is apparent that the optimized directions give better results both visually and in terms of reconstruction error as shown in Fig. 14. Results for more materials and different numbers of rotations are shown in the supplementary material.

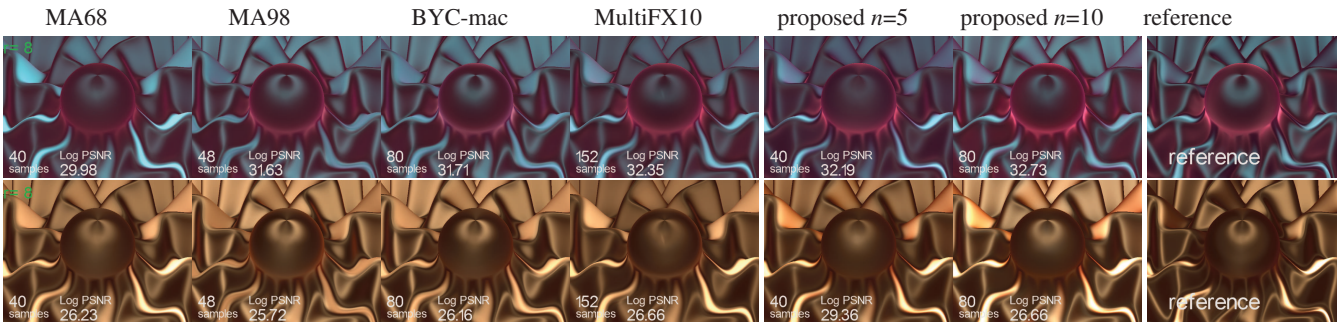


**Figure 14:** *BRDF reconstruction from $r = 8$ rotations using bidirectional geometries of four industrial devices when compared to the proposed optimized sampling using $n = 5, 10$ samples per rotation. Included are values of Log PSNR error and total number of samples.*

These results demonstrate that although current available multi-angle reflectance measurement devices are designed primarily to discriminate materials and their visual properties, they can be, when combined with a rotation stage for material positioning, readily used for the capturing of main features of anisotropic BRDFs. However, whenever a higher accuracy is needed, one should resort to a custom build apparatus with ten or more bidirectional pairs optimized to anisotropic behavior. Still such a device could capture and reconstruct anisotropic BRDF in several minutes.

## 8. Conclusion

This paper outlines a method for the convenient acquisition of anisotropic BRDFs while relying on an extremely low number of samples. The method allows measurement decomposition into several independent azimuthal slices sharing the same bidirectional geometry. Such geometry consists of between five to ten bidirectional pairs, either repositioned around measured material or the material rotating below. The total number of samples is given by a product of geometric complexity (i.e., number of bidirectional pairs) and number of rotations. We show that below one hundred samples are sufficient to capture main features of even highly anisotropic materials. To further improve the performance of our method, we extended it to adaptive sampling of anisotropy. Finally, we have shown that our method can directly utilize current industrial multi-angle reflectometers for the convenient measurement of approximate anisotropic BRDFs. Our method relies on a linear basis consisting of a training database of anisotropic materials. As a part of this paper are provided codes for linear basis construction, optimization of sampling directions, and BRDF reconstruction at http://staff.utia.cas.cz/filip/projects/16PG/.

In a future work we plan to improve descriptiveness of our linear basis and thus further reduce reconstruction error by collecting additional isotropic and anisotropic BRDFs from various sources.

## Acknowledgments

This research has been supported by the Czech Science Foundation grant 14-02652S.

## References

[AMS08] AYDIN T. O., MANTIUK R., SEIDEL H.-P.: Extending quality metrics to full luminance range images, 2008. 6

[BEWW*08] BEN-EZRA M., WANG J., WILBURN B., LI X., MA L.: An LED-only BRDF measurement device. *Computer Vision and Pattern Recognition, IEEE Computer Society Conference on 0* (2008), 1–8. 3

[BMVS04] BLANZ V., MEHL A., VETTER T., SEIDEL H. P.: A statistical method for robust 3D surface reconstruction from sparse data. In *Proceedings of 2nd International Symposium on 3D Data Processing, Visualization and Transmission* (2004), pp. 293–300. 5

[BNS78] BUNCH J. R., NIELSEN C. P., SORENSEN D. C.: Rank-one modification of the symmetric eigenproblem. *Numerische Mathematik 31*, 1 (1978), 31–48. 12

[DW04] DANA K., WANG J.: Device for convenient measurement of spatially varying bidirectional reflectance. *Journal of Optical Society of America 21*, 1 (2004), 1–12. 3

[FBLS07] FUCHS M., BLANZ V., LENSCH H. P., SEIDEL H.-P.: Adaptive sampling of reflectance fields. *ACM Trans. Graph. 26* (June 2007), 1–18. 4

[Fil15] FILIP J.: Analyzing and predicting anisotropic effects of BRDFs. In *Proceedings of the ACM SIGGRAPH Symposium on Applied Perception* (2015), SAP '15, pp. 25–32. 4

[FSH16] FICHET A., SATO I., HOLZSCHUCH N.: Capturing spatially varying anisotropic reflectance parameters using fourier analysis. In *Graphics Interface 2016* (2016). 4

[FV14] FILIP J., VAVRA R.: Template-based sampling of anisotropic BRDFs. *Computer Graphics Forum (PG 2014) 33*, 7 (2014), 91–99. 3, 4, 7, 9

[FVH*13] FILIP J., VAVRA R., HAINDL M., ZID P., KRUPICKA M., HAVRAN V.: BRDF slices: Accurate adaptive anisotropic appearance acquisition. In *CVPR* (2013), pp. 4321–4326. 3

[FVH14] FILIP J., VÁVRA R., HAVLICEK M.: Effective acquisition of dense anisotropic BRDF. In *Proceedings of the 22th International Conference on Pattern Recognition, ICPR 2014* (August 2014), pp. 2047–2052. 3

[GHAO10] GHOSH A., HEIDRICH W., ACHUTHA S., OÏ£¡TOOLE M.: A basis illumination approach to BRDF measurement. *International Journal of Computer Vision 90*, 2 (2010), 183–197. 3

[Gol73] GOLUB G. H.: Some modified matrix eigenvalue problems. *Siam Review 15*, 2 (1973), 318–334. 12

[HFM10] HAVRAN V., FILIP J., MYSZKOWSKI K.: Bidirectional texture function compression based on the multilevel vector quantization. *Computer Graphics Forum 29*, 1 (2010), 175–190. 3

[HFM16] HAVRAN V., FILIP J., MYSZKOWSKI K.: Perceptually motivated BRDF comparison using single image. *Computer Graphics Forum (Proceedings of EGSR) 35* (2016), 1–12. 6

[HLZ10] HOLROYD M., LAWRENCE J., ZICKLER T.: A coaxial optical scanner for synchronous acquisition of 3D geometry and surface reflectance. *ACM Trans. Graph. 29* (2010), 99:1–99:12. 3

[HP03] HAN J., PERLIN K.: Measuring bidirectional texture reflectance with a kaleidoscope. *ACM SIGGRAPH 2003 22*, 3 (2003), 741–748. 3

[LL95] LU J., LITTLE J.: Reflectance function estimation and shape recovery from image sequence of a rotating object. In *Proceedings of the Fifth International Conference on Computer Vision* (Washington, DC, USA, 1995), ICCV '95, IEEE Computer Society, pp. 80–. 3

[LLSS03] LENSCH H. P., LANG J., SÁ A. M., SEIDEL H.-P.: Planned sampling of spatially varying BRDFs. *Computer Graphics Forum 22*, 3 (2003), 473–482. 4

[MPBM03a] MATUSIK W., PFISTER H., BRAND M., MCMILLAN L.: A data-driven reflectance model. *ACM Transactions on Graphics 22*, 3 (2003), 759–769. 3, 4, 9

[MPBM03b] MATUSIK W., PFISTER H., BRAND M., MCMILLAN L.: Efficient isotropic BRDF measurement. In *Proceedings of the 14th Eurographics Workshop on Rendering* (2003), pp. 241–247. 4, 6, 7

[NDM05] NGAN A., DURAND F., MATUSIK W.: Experimental analysis of BRDF models. *Eurographics Symposium on Rendering 2005 2* (2005), 117–126. 3

[NFM14] NAUYOKS S. E., FREDA S., MARCINIAK M. A.: Dynamic data driven bidirectional reflectance distribution function measurement system, 2014. 4

[NJR15] NIELSEN J. B., JENSEN H. W., RAMAMOORTHI R.: On Optimal, Minimal BRDF Sampling for Reflectance Acquisition. *ACM Trans. Graph. 34*, 6 (2015), 186:1–186:11. 3, 4, 5, 6, 7, 9

[NKS14] NÖLL T., KÖHLER J., STRICKER D.: Robust and accurate non-parametric estimation of reflectance using basis decomposition and correction functions. In *ECCV (LNCS 8690)* (2014), pp. 376–391. 4

[NRH*77] NICODEMUS F., RICHMOND J., HSIA J., GINSBURG I., LIMPERIS T.: Geometrical considerations and nomenclature for reflectance. *NBS Monograph 160* (1977), 1–52. 2

[PCVMV13] PERALES E., CHORRO E., VIQUEIRA V., MARTÍNEZ-VERDÚ F. M.: Reproducibility comparison among multiangle spectrophotometers. *Color Research & Applic. 38*, 3 (2013), 160–167. 10

[Rus98] RUSINKIEWICZ S.: A new change of variables for efficient BRDF representation. In *Rendering techniques' 98* (1998), pp. 11–22. 3

[SAS05] STARK M., ARVO J., SMITS B.: Barycentric parameterizations for isotropic BRDFs. *IEEE TVCG 11*, 2 (2005), 126 –138. 3

[WM01] WESTLUND H. B., MEYER G. W.: Applying appearance standards to light reflection models. In *Proceedings of the 28th Annual Conference on Computer Graphics and Interactive Techniques* (2001), SIGGRAPH '01, pp. 501–51. 10

[XSD*13] XU K., SUN W.-L., DONG Z., ZHAO D.-Y., WU R.-D., HU S.-M.: Anisotropic spherical gaussians. *ACM Trans. Graph. 32*, 6 (2013), 209:1–209:11. 4

[YSY32] YASUHIRO M., SUMINO K., YASUSHI Y.: Rapid BRDF measurement using an ellipsoidal mirror and a projector. *IPSJ Trans. on Computer Vision and Appl. 1* (21–32). 3

## Appendix A: Gradient of the Objective Function

$$\begin{aligned}
E(\boldsymbol{C}) &= \|\tilde{\boldsymbol{Y}} - \tilde{\boldsymbol{Q}}\boldsymbol{C}\|_F^2 + \eta\|\boldsymbol{C}\|_F^2 + \lambda\|\tilde{\tilde{\boldsymbol{Q}}}\boldsymbol{C}\boldsymbol{M}\|_F^2 \\
\nabla E(\boldsymbol{C}) &= \nabla\|\tilde{\boldsymbol{Y}} - \tilde{\boldsymbol{Q}}\boldsymbol{C}\|_F^2 + \eta\nabla\|\boldsymbol{C}\|_F^2 + \lambda\nabla\|\tilde{\tilde{\boldsymbol{Q}}}\boldsymbol{C}\boldsymbol{M}\|_F^2 \\
&= \nabla\,\mathrm{Tr}[(\tilde{\boldsymbol{Y}} - \tilde{\boldsymbol{Q}}\boldsymbol{C})^T(\tilde{\boldsymbol{Y}} - \tilde{\boldsymbol{Q}}\boldsymbol{C})] + \eta\nabla\,\mathrm{Tr}(\boldsymbol{C}^T\boldsymbol{C}) + \\
&\quad \lambda\nabla\,\mathrm{Tr}[(\tilde{\tilde{\boldsymbol{Q}}}\boldsymbol{C}\boldsymbol{M})^T(\tilde{\tilde{\boldsymbol{Q}}}\boldsymbol{C}\boldsymbol{M})] \\
&= \nabla\,\mathrm{Tr}(\tilde{\boldsymbol{Y}}^T\tilde{\boldsymbol{Y}}) - \nabla\,\mathrm{Tr}(\boldsymbol{C}^T\tilde{\boldsymbol{Q}}^T\tilde{\boldsymbol{Y}}) - \nabla\,\mathrm{Tr}(\tilde{\boldsymbol{Y}}^T\tilde{\boldsymbol{Q}}\boldsymbol{C}) + \\
&\quad \nabla\,\mathrm{Tr}(\boldsymbol{C}^T\tilde{\boldsymbol{Q}}^T\tilde{\boldsymbol{Q}}\boldsymbol{C}) + \eta\nabla\,\mathrm{Tr}(\boldsymbol{C}^T\boldsymbol{C}) + \\
&\quad \lambda\nabla\,\mathrm{Tr}(\boldsymbol{M}\boldsymbol{C}^T\tilde{\tilde{\boldsymbol{Q}}}^T\tilde{\tilde{\boldsymbol{Q}}}\boldsymbol{C}\boldsymbol{M}) \\
&= -2\tilde{\boldsymbol{Q}}^T\boldsymbol{Y} + 2\tilde{\boldsymbol{Q}}^T\tilde{\boldsymbol{Q}}\boldsymbol{C} + 2\eta\boldsymbol{C} + 2\lambda\tilde{\tilde{\boldsymbol{Q}}}^T\tilde{\tilde{\boldsymbol{Q}}}\boldsymbol{C}\boldsymbol{M}\boldsymbol{M}.
\end{aligned}$$

## Appendix B: Fast Update of the Condition Number

Let $\tilde{\boldsymbol{Q}} \in \mathbb{R}^{n\times k}$ be the selected rows of the principal components in $\boldsymbol{Q}$, whose condition number we are seeking for. Condition number is defined as $\kappa(\tilde{\boldsymbol{Q}}) = \frac{\sigma_{max}(\tilde{\boldsymbol{Q}})}{\sigma_{min}(\tilde{\boldsymbol{Q}})}$, i.e., the ratio between the maximum and minimum singular values of $\tilde{\boldsymbol{Q}}$. Note that singular values of $\tilde{\boldsymbol{Q}}$ are equal to the square roots of the eigenvalues of the matrix $\tilde{\boldsymbol{Q}}^T\tilde{\boldsymbol{Q}}$. Therefore, we can exploit methods for fast update of eigenvalues when rank-one modification of the matrix were performed [BNS78]. Let $\bar{\boldsymbol{Q}} \in \mathbb{R}^{n-1\times k}$ be the desired matrix $\tilde{\boldsymbol{Q}}$ with one row removed. Specifically, without loss of generality, we can write

$$\tilde{\boldsymbol{Q}} = \begin{bmatrix}\bar{\boldsymbol{Q}}\\ \boldsymbol{q}^T\end{bmatrix}, \quad \tilde{\boldsymbol{Q}}^T\tilde{\boldsymbol{Q}} = \begin{bmatrix}\bar{\boldsymbol{Q}}^T\boldsymbol{q}\end{bmatrix}\begin{bmatrix}\bar{\boldsymbol{Q}}\\ \boldsymbol{q}^T\end{bmatrix} = \bar{\boldsymbol{Q}}^T\bar{\boldsymbol{Q}} + \boldsymbol{q}\boldsymbol{q}^T,$$

where $\boldsymbol{q}^T \in \mathbb{R}^{1\times k}$ is a row of $\boldsymbol{Q}$, which we are adding to current matrix $\bar{\boldsymbol{Q}}$. Obviously, we want to select such a $\boldsymbol{q}^T$, that $\kappa(\tilde{\boldsymbol{Q}})$ is minimum.

Let $\rho = \|\boldsymbol{q}\|_2^2$ and $\boldsymbol{b} = \frac{1}{\sqrt{\rho}}\boldsymbol{q}$. Then $\tilde{\boldsymbol{Q}}^T\tilde{\boldsymbol{Q}} = \bar{\boldsymbol{Q}}^T\bar{\boldsymbol{Q}} + \rho\boldsymbol{b}\boldsymbol{b}^T$ and we can once solve the symmetric eigenproblem of $\bar{\boldsymbol{Q}}^T\bar{\boldsymbol{Q}} = \boldsymbol{V}\boldsymbol{D}\boldsymbol{V}^T$, where $\boldsymbol{D} \in \mathbb{R}^{k\times k}$ is diagonal matrix of eigenvalues and $\boldsymbol{V} \in \mathbb{R}^{k\times k}$ is matrix of corresponding eigenvectors. Now, we can write $\bar{\boldsymbol{Q}}^T\bar{\boldsymbol{Q}} + \rho\boldsymbol{b}\boldsymbol{b}^T = \boldsymbol{V}(\boldsymbol{D} + \rho\boldsymbol{z}\boldsymbol{z}^T)\boldsymbol{V}^T$, where $\boldsymbol{z} = \boldsymbol{V}^T\boldsymbol{b}$. Let $\boldsymbol{C} = \boldsymbol{D} + \rho\boldsymbol{z}\boldsymbol{z}^T = \boldsymbol{X}\tilde{\boldsymbol{D}}\boldsymbol{X}^T$. Then $\tilde{\boldsymbol{Q}}^T\tilde{\boldsymbol{Q}} = \tilde{\boldsymbol{V}}\tilde{\boldsymbol{D}}\tilde{\boldsymbol{V}}^T$, where $\tilde{\boldsymbol{V}} = \boldsymbol{V}\boldsymbol{X}$, but we are only interested in maximum and minimum eigenvalue of $\tilde{\boldsymbol{D}}$ to compute $\kappa(\tilde{\boldsymbol{Q}})$.

Let $d_1 \le d_2 \le \cdots \le d_k$ be the eigenvalues of $\boldsymbol{D}$ and let $\tilde{d_1} =\le \tilde{d_2} \le \cdots \le \tilde{d_k}$ be the eigenvalues of $\boldsymbol{C}$ (and therefore also of $\tilde{\boldsymbol{D}}$). Then holds $d_1 \le \tilde{d_1} \le d_2$ and $d_k \le \tilde{d_k} \le d_k + \rho$. Golub [Gol73] has shown that this eigenvalues can be computed by finding zeros of the secular equation

$$w(\tilde{d_i}) = 1 + \rho\sum_{j=1}^{k}\frac{z_j^2}{d_j - \tilde{d_i}},$$

where $\boldsymbol{z} = [z_1,\ldots,z_k]^T$. The equation can be solved numerically by bisection method. First, we set lover bound of an interval to $d_1$ and upper bound to $d_2$ and we find $\tilde{d_1}$ in the interval where $w(\tilde{d_1}) \le \varepsilon$ for sufficiently small $\varepsilon$. Second, we set lover bound to $d_k$ and upper bound to $d_k + \rho$ and perform the bisection method once again to find $\tilde{d_k}$ in the interval where $w(\tilde{d_k}) \le \varepsilon$. In praxis, we perform interval subdivision 30-times achieving very precise results.

Condition number of the updated matrix $\tilde{\boldsymbol{Q}}$ is finally computed as $\kappa(\tilde{\boldsymbol{Q}}) = \frac{\sqrt{\tilde{d_k}}}{\sqrt{\tilde{d_1}}}$.